Organic Electronics 52 (2018) 79–88

Contents lists available at ScienceDirect

Organic Electronics

journal homepage: www.elsevier.com/locate/orgel

Interface state contribution to the photovoltaic effect in organic phototransistors: Photocapacitance measurements and optical sensing

C.P. Watson[a], E.M. Lopes[a,1], R.F. de Oliveira[b], N. Alves[c], J.A. Giacometti[d], D.M. Taylor[a,*]

[a] School of Electronic Engineering, Bangor University, Dean Street, Bangor, Gwynedd, LL57 1UT, UK
[b] Brazilian Nanotechnology National Laboratory (LNNano), Brazilian Centre of Research in Energy and Materials (CNPEM), CEP 13083-970, Campinas, São Paulo, Brazil
[c] Department of Physics, São Paulo State University (UNESP), PO Box 266, CEP 19060-900, Presidente Prudente, São Paulo, Brazil
[d] Institute of Physics of São Carlos, University of São Paulo (USP), PO Box 369, CEP 13560-970, São Carlos, São Paulo, Brazil

ARTICLE INFO

Keywords:
Photocapacitance
Interface states
Phototransistors
Photovoltaic effect
poly(3-hexylthiophene)

ABSTRACT

We report the results of an investigation into the contribution that trapping in interface states makes to the photovoltaic effect observed in organic phototransistors. To isolate this effect from other processes that occur in the transistor structure when under illumination, we focus attention on the photo-response of metal-insulator-semiconductor (MIS) capacitors - the core structure of transistors. The capacitors comprised poly(3-hexylthiophene), (P3HT), as the active semiconductor in combination with one of three insulators, namely, poly (amide-imide), (PAI), SU-8 photoresist and polysilsesquioxane (PSQ). Following initial characterization in the dark, the capacitor response was measured both during and after irradiation with light in the wavelength range 400–700 nm. Three different approaches were employed to study the photo-response, each providing a different insight into the processes occurring. Capacitance-voltage sweeps before, during and after illumination provided direct evidence supporting the view that the photovoltaic effect occurred as a result of electron trapping in interface states of density up to $\sim 2 \times 10^{12}$ cm^{-2} in the P3HT/PAI combination but lower for SU-8 and PSQ. The dynamic photo-response, in which device capacitance was held constant by changing the applied bias, showed a fast component related to optically induced photoconduction in the semiconductor and a slower component reflecting the dynamics of interface electron trapping. Finally, photo-induced capacitance changes occurring with constant applied voltage were used to demonstrate a simple 3 × 3 imaging array.

1. Introduction

Organic imaging arrays formed on flexible substrates are attracting considerable interest, particularly for large-area imaging systems [1,2]. In their comprehensive review [2], Pierre and Arias describe the operation of pixel arrays based on photodiodes and phototransistors. They also provide figures of merit for the various technologies, thereby highlighting the potential of solution-processed organic materials for such systems. To further emphasise the possibilities presented by organics, Pierre et al. [3] recently reported a novel phototransistor structure incorporating a donor-acceptor bulk heterojunction (BHJ) film as the photosensitive layer underlying a high-mobility p-type organic semiconductor dinaphtho[2,3-b:2′,3′-f]thieno[3,2-*b*]thiophene (DNTT). During the 'sense' operation, photo-generated holes were injected into the DNTT leaving electrons trapped in the BHJ to be neutralised during the 'reset' operation. This is similar to the structure described by Zhang et al. [4] in which photo-generated electrons in pentacene were injected into an electron trapping layer causing a shift in the threshold voltage, V_T. In the latter case, electrons remained trapped for long periods in the layer, > 20,000 s, or were erased by briefly turning on the transistor structure with a high voltage pulse. In conventional organic phototransistors, the optical response is usually attributed to two mechanisms, namely the photoconduction and the photovoltaic effects.

In photoconduction, charge carriers photo-generated in the bulk semiconductor give rise to a current flow parallel to the conventional channel current of the transistor. It is generally observed in the OFF-state of the transistor [1,5,6], although a model has been developed for photoconduction in the saturation regime [7].

The photovoltaic effect arises when illumination causes a significant shift in V_T. This effect is most obvious in the subthreshold regime of operation where small photo-induced changes in V_T lead to orders of

* Corresponding author.
E-mail address: d.m.taylor@bangor.ac.uk (D.M. Taylor).
[1] Present address: Catarinense Federal Institute of Education, Science and Technology, PO Box 21, CEP 89245-000, Araquari, Santa Catarina, Brazil.

http://dx.doi.org/10.1016/j.orgel.2017.10.010
Received 9 August 2017; Received in revised form 4 October 2017; Accepted 7 October 2017
Available online 10 October 2017
1566-1199/ © 2017 Elsevier B.V. All rights reserved.

magnitude change in channel current and hence high responsivity. In this contribution, we concentrate attention on this latter mechanism.

We begin with a brief review of models proposed for the photovoltaic effect and then show how photocapacitance measurements can be used to identify shifts in threshold voltage that arise specifically from charge trapping in interface states. Finally, we demonstrate how the photocapacitance effect can be used for imaging.

2. Origin of the photovoltaic effect

There is some debate as to the origin of the V_T shift in phototransistors. Wasapinyokul et al. [7] describe a model showing that, under illumination, the intrinsic V_T is unchanged from its dark value. Rather the photo-induced shift is a consequence of the photocurrent contribution. However, the model appears to be limited to a semiconductor with balanced hole and electron mobilities, an uncommon situation.

Based on an explanation given for metamorphic, high electron mobility inorganic phototransistors [8–10], a number of authors [1,2,5,6] suggest that photo-generated electrons become trapped in the channel region close to the source contact thus reducing V_T and enhancing hole injection. It is not clear, however, why a mathematical description for these metamorphic structures is applicable to organic phototransistors. Additionally, in the latter case, the work function of the source electrode is chosen to match as closely as possible the highest occupied molecular orbital (HOMO) of the organic semiconductor. The energetics should favour, therefore, the transfer of electrons into the electrode, over their trapping in the semiconductor.

In the transistor OFF-state, the strongest electric fields are normal to the plane of the insulator/semiconductor interface. Consequently, electrons present in the semiconductor will be attracted to that interface rather than drift to the source in a direction parallel to the channel. That a higher photo-response is often observed when the transistor is biased into saturation [1,5] is consistent, though, with electron trapping in the semiconductor near the source contact. However, this view neglects the effect of light on the electron quasi Fermi level (QFL), which moves closer to the lowest unoccupied molecular orbital (LUMO) with increasing light intensity. A higher electron QFL at the interface will result in more interface electron traps becoming active, even when band-bending appears unfavourable as is the case when a p-channel transistor is turned on. Although this particular mechanism is not discussed, nevertheless, many authors [1,6,11–13] ascribe the shift in V_T to electron trapping at the semiconductor/insulator interface or in the insulator itself. Identified sources of electron traps in or on the surface of gate insulators include water-related hydroxyl groups on silicon oxide [13], hydroxyl moieties on polymers such as polyvinylphenol [12], other polar groups in the gate polymer, e.g. in a polylactide biopolymer [14], and structural defects in, for example, aluminium oxide [11].

It is well-known [15,16] that, charge trapping at the semiconductor/insulator interface or in the insulator itself causes a shift, ΔV_{FB}, in the flat-band voltage given by $\Delta V_{FB} = -Q_{it}/C_i$, where Q_{it} is the effective density of interface trapped charge and C_i the insulator capacitance per unit area. In the presence of interface or insulator trapped charge, therefore, the conventional equation for the transistor current, I_D, must be written in terms of an effective threshold voltage, $V_T(eff) = (V_T + \Delta V_{FB}) = (V_T - Q_{it}/C_i)$, so that

$$I_D = \frac{W}{L}\mu C_i\left[\left(V_G - V_T + \frac{Q_{it}}{C_i}\right) - \frac{V_D}{2}\right]V_D \quad (1)$$

where I_D is the channel current, W and L the channel width and length respectively, μ the mobility and V_G and V_D the gate and drain voltages respectively. Thus, the main effect of photo-induced electron trapping in interface states (Q_{it} is then a negative quantity) is simply to shift the transfer characteristic of a p-channel device towards less negative gate voltages, without change of shape [15,16], thus increasing channel current for particular values of V_G. The detailed shape of the transfer characteristic obtained under illumination may depend, though, on a number of secondary factors. For example, the dynamics of interface charge trapping and release could result in different characteristics being obtained depending on (a) whether the gate voltage sweep begins from the OFF rather than ON state, (b) using different voltage sweep rates and (c) the wavelength and intensity of the incident radiation. Through coulombic interactions, interface trapped charges could also reduce carrier mobility in the channel while the OFF current under illumination, determined by the bulk photocurrent, could be much higher, i.e. the photoconductive effect.

In silicon technology, interface charge trapping has been widely investigated using metal-insulator-semiconductor (MIS) capacitors [15,16], the core structure of thin film transistors. In MIS capacitors, applied electric fields and the resulting transient electron/hole current flows are perpendicular to the plane of the device. Consequently, their electrical characteristics are not complicated by channel or bulk currents flowing parallel to the semiconductor/insulator interface as occurs in transistors. By monitoring changes in the capacitance-voltage (*C-V*) plots of MIS capacitors during and after illumination, unambiguous evidence may be obtained for the influence of interface charge trapping on ΔV_{FB} and hence the contribution made to the photovoltaic effect in the various semiconductor/insulator combinations used in transistors. For example, MIS capacitors based on poly(3-hexylthiophene), P3HT, as the active semiconductor and a range of insulators e.g. polyimide [17], polysilsesquioxane (PSQ) [17], atomic layer deposited aluminium titanium oxide [18] and SU-8 photoresist [19] show very different behaviours. A range of effects, all of which can be attributed to interface charging, has been observed in photocapacitance measurements, even when using the same semiconductor. As concluded from studies of phototransistors with different insulators [12], this clearly points to the importance of the insulator layer in determining the extent of the photo-induced shift in V_T as well as the lifetime of the photo-response after terminating the illumination.

In the following, we present new results, which demonstrate the ability of the photocapacitance technique to identify those features of phototransistor response that arise specifically from interface trapping. For this purpose, solution-processed organic MIS capacitors based on P3HT as the semiconductor and three different insulators, namely, poly (amide-imide) (PAI), SU-8 photoresist and PSQ, have been fabricated and evaluated. Three different approaches for investigating the role of interface states have been explored based on (i) photocapacitance-voltage sweep, (ii) time-dependent photo-response, and (iii) light-induced capacitance changes with constant applied voltage. Finally, via a simple capacitor array, we demonstrate how the photocapacitance effect could be used as the basis of an imaging device.

3. Experimental

3.1. Materials

To prepare MIS capacitors (Fig. 1(a)), indium-tin-oxide (ITO) coated glass slides (sheet resistance 15–25 Ω/square, purchased from Delta Technologies) were used as transparent bottom electrodes. The insulating polymer poly(amide-imide), PAI, was synthesized as previously reported in the literature [20]. SU-8 photoresist was purchased from Microchem Ltd, the PSQ precursor (90% phenyl and 10% methyl) from Gelest Inc and P3HT, regioregularity > 98.5%, M_W = 87,000 g/mol, from Sigma-Aldrich and used without further purification.

3.2. MIS capacitor fabrication

The different insulating layers were prepared on ITO substrates previously cleaned using deionized water, detergent and sonication in a solution of 20% (v/v) of ethanolamine in ultrapure water for 20 min,

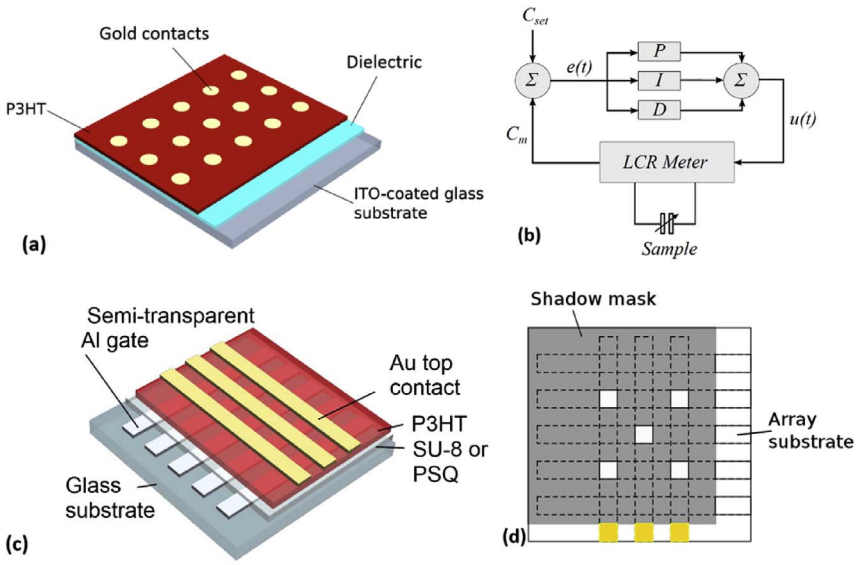

Fig. 1. (a) MIS capacitors used for photocapacitance measurements. (b) The PID circuit used for tracking the shift in threshold voltage. (c) Capacitor imaging array and (d) the shadow mask attached to the underside of the glass substrate for demonstrating the imaging principle.

following the manufacturer's recommended procedure. The PSQ film was spin-coated at 1000 rpm for 60 s from 80 mg/mL precursor solution prepared in butanone. In a curing protocol developed for this work, the deposited film was heated on a hotplate at 100 °C for 30 min, then a further 30 min at 150 °C followed by a 24 h bake in a vacuum oven (10^{-2} Torr) at 180 °C. Previously reported methods were used to prepare the PAI [20] and SU-8 [19] films. Briefly, PAI was spin-coated from a mixture of N-methyl-pyrrolidone and xylene and cured under vacuum for 15 h at 200 °C, yielding films ~300 nm thick. SU-8 films ranging from ~100 to ~200 nm thick were spin-coated from cyclopentanone followed by a pre-bake, UV cure and post-bake. P3HT films were spin-coated from solutions in chloroform in a nitrogen glove-box. In each case, the insulating layer was treated with a hexmethyldisilazane (HMDS) self-assembled monolayer (SAM) prior to P3HT deposition in order to improve ordering of the molecular layers adjacent to the insulator surface [21]. The MIS capacitors, see Fig. 1(a), were completed by depositing circular gold electrodes (2 mm in diameter and 60-70 nm-thick) by thermal evaporation (Edwards Coating System Auto 306) using a shadow mask.

Prior to making measurements, the excess P3HT film around the top electrodes was carefully removed by mechanical scribing to minimise possible lateral current effects [22,23]. Then, to remove solvent traces and any adventitious P3HT dopants (e.g. atmospheric oxygen) introduced during sample preparation, the devices were mounted in a sample holder and heated up to 100 °C for 1 h under high vacuum (~10^{-6} Torr) with the electrical contacts short-circuited. After this conditioning procedure, the devices were cooled to room temperature and electrical characterization undertaken without breaking the vacuum.

3.3. Photocapacitance measurements

Admittance measurements were made under vacuum using a Frequency Response Analyser (Solartron, model 1255) combined with the 1296 Dielectric Interface accessory. The small-signal amplitude was 100 mV. Firstly, the capacitance, C, and dielectric loss, G/ω, (conductance/angular frequency) of all devices were measured as a function of frequency (C-f and G/ω-f) to determine the onset of the Maxwell-Wagner dispersion [20,24,25]. This was necessary to ensure that capacitance-voltage (C-V) plots were measured at a frequency set sufficiently low, typically < 400 Hz, to avoid effects related to this dispersion. For these latter measurements, the bias voltage, V, was applied to the ITO electrode, and swept from negative to positive values and back again, typically at a rate of 100 mV/s. Photocapacitance measurements were made using a xenon discharge lamp coupled to a Jobin Yvon Triax 320 monochromator. The latter was set at a wavelength $\lambda = 500$ nm, which is close to the maximum absorption in P3HT [19]. Monochromatic light was transmitted into the cryostat through a quartz window and illuminated the devices through the ITO bottom electrode. The incident light intensity, typically ~1 W/m^2 at the device position, was measured with a sensor (Anritsu model MA9411A1) coupled to a power meter (Anritsu model M-9001A). The experimental conditions above, including the maximum voltage applied, were chosen based on a previously reported detailed study of the effect of incident radiation and voltage sweep rate on such capacitors [19]. The conditions are such as to allow the discrimination of different effects in the various samples within the timescale determined by the voltage sweep rate.

When investigating the time-dependence of the optical response in phototransistors and MIS capacitors, charging/discharging of interface states during the measurement changes the degree of band bending at the semiconductor/insulator interface. This in turn changes the dynamics of charge trapping/de-trapping making it more difficult to interpret the resulting data. To overcome this, we undertook measurements in which band bending was maintained constant during illumination, and afterwards in the dark, by adjusting the applied voltage using a proportional-integral-derivative (PID) controller in conjunction with a LCR meter (Fig. 1(b)) to maintain a constant measured capacitance set at a value corresponding to partial depletion of the P3HT. We have used this technique previously to track the recovery of the flatband voltage after illuminating P3HT MIS capacitors formed on polyimide and PSQ [17].

Based on phototransistor measurements, e.g. Ref. [11], the response time of the measurement system, ~ few seconds, was deemed to be short enough to follow the dynamic processes. Thus at each wavelength, devices were illuminated for 60 s followed by a 60 s period in the dark. With incident light intensity ~0.2 W/m^2 this time scale was sufficient for the trapping/detrapping dynamics to be established with reasonable accuracy. Furthermore, the trapped electron density after each successive light-dark period remained well below the total trap density. Thus, the residual electrons still in trap states at the start of the subsequent illumination period would have minimal effect on the corresponding dynamic response.

However, as will be seen later, the true time-constant of a fast component in the optical response related to a photoconductive process in P3HT could not be determined.

3.4. Fabrication and testing of an imaging demonstrator

MIS capacitor arrays with the structure shown in Fig. 1(c) were fabricated following the protocols described above for the individual MIS capacitors. The only differences were: (a) The bottom electrodes were now five vacuum-evaporated co-planar, 20 nm thick, 2 mm wide, semi-transparent aluminium stripes separated by a 4 mm gap. (b) The top electrodes were formed by vacuum-evaporating three orthogonal, 20 nm thick gold stripes, again 2 mm wide and separated by a 4 mm gap, resulting in a 5 × 3 capacitor matrix. After conditioning, admittance measurements were made to check the functionality of each capacitor in the array. Owing to the limited number of connections into the cryostat, testing the whole array as an 'imaging' device was performed under ambient conditions with only the central 3 × 3 array used.

To ensure identical electro-optical conditions during illumination, the aluminium electrodes were connected together, similarly the gold electrodes, thus forming one large capacitor. After careful alignment of the optical shadow mask (Fig. 1(d)) on the underside of the glass substrate, a positive voltage was applied to the aluminium electrodes for 1 min with the gold held at ground. Simultaneously, white light from a fluorescent lamp (850 lux at the device position) illuminated the array through the mask. With the electrodes uncoupled, the capacitance of each capacitor was measured in the dark as a function of time and with the applied voltage set to a value corresponding to the beginning of the minimum capacitance plateau observed during the initial dark measurement.

4. Results and discussion

4.1. Comparison of pre- and post-illumination C-V plots

C-V plots for P3HT-based MIS capacitors on (a) PAI, (b) SU-8 and (c) PSQ gate insulators are given in Fig. 2. These were obtained initially in the dark, then during illumination with 500 nm light and finally in the dark immediately after illumination. The arrows indicate the counter-clockwise hysteresis seen in all the devices, especially under illumination. For negative bias in the dark, the devices are in accumulation with capacitance values corresponding to the insulator capacitance, C_I. The lower value for PSQ reflects the thicker layer in this case.

For positive bias, V_G, the semiconductor depletes and the capacitance falls following a relation of the form [15].

$$\frac{C_I}{C} = \sqrt{1 + \frac{2C_I^2}{qA^2N_A\varepsilon_S}(V_G - V_{FB})} \quad (2)$$

where q is the electronic charge, V_{FB} the flatband voltage which accounts for the effective density of interface trapped charge and any work function difference between the semiconductor and the metal contact to the insulator. A is the device area, with N_A and ε_S, respectively, the doping density and absolute permittivity of the semiconductor. At sufficiently high positive voltages, the P3HT layer is fully depleted with the capacitance attaining a constant minimum value, C_{min}, corresponding to the series sum of the insulator and semiconductor capacitances, C_I and C_S respectively.

The doping density, N_A, in the P3HT was determined for each case from the slope of the *C-V* data replotted in Mott-Schottky format, i.e. C^{-2} vs V_G. Values of N_A extracted from the linear sections of plots corresponding to the first forward voltage sweep in the dark are given in Table 1. For the PSQ devices, N_A is typical of values reported previously [25] i.e. $< 10^{16}$ cm^{-3}, and is likely to be due to oxidative/photo-oxidative reactions from exposure to atmospheric oxygen or ozone [26,27]. The higher values in the PAI and SU-8 devices suggest that, during spin-coating, additional impurities such as initiators and/or low molecular weight fragments may have leached out from the insulator into the P3HT. Such impurities, and possibly atmospheric oxygen, may not have been removed completely during vacuum-annealing of the final device.

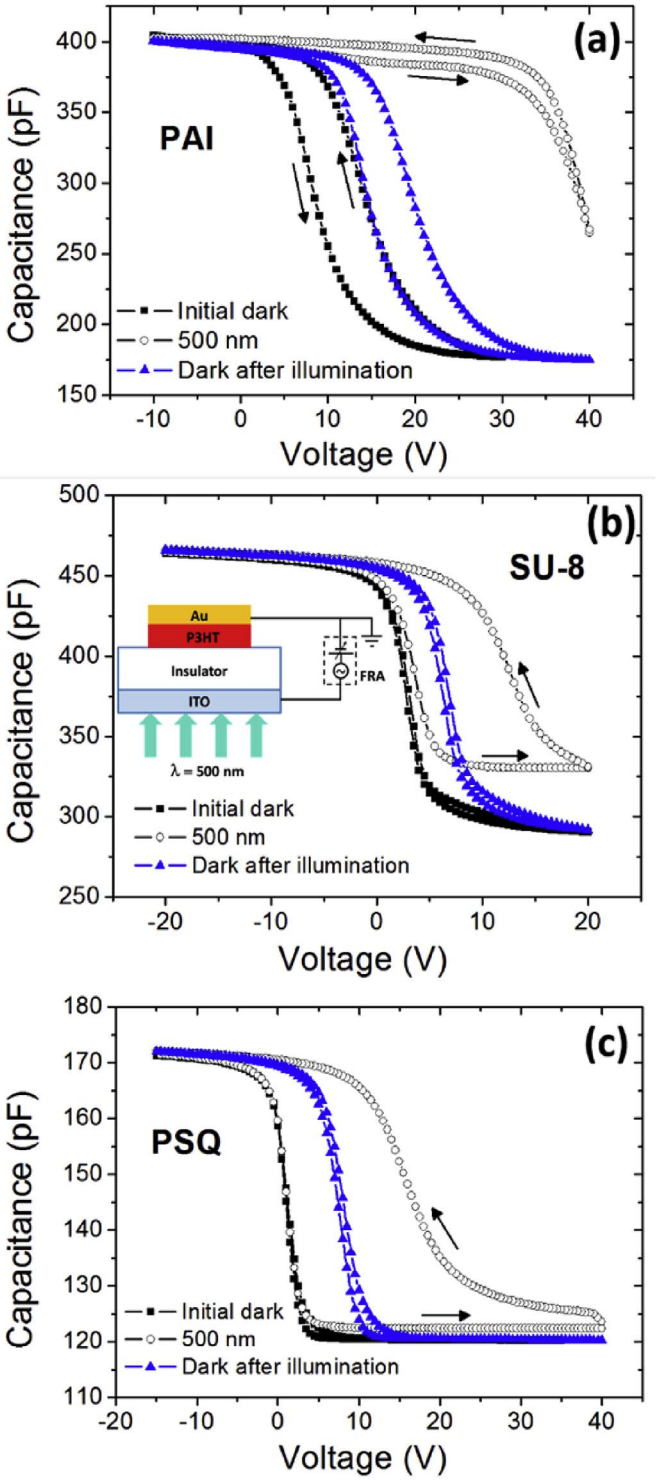

Fig. 2. *C-V* plots obtained for P3HT MIS capacitors based on the insulators (a) PAI, (b) SU-8 and (c) PSQ obtained before, during and after illumination with 500 nm light. The inset in (b) shows the experimental arrangement.

Interestingly, only devices formed on PAI exhibited significant hysteresis in the *C-V* plots collected in the dark. For all device types, V_{FB} - typically $\sim 0.9C_I$ in doped semiconductors - is close to 0 V during the initial forward voltage sweep. The counter-clockwise hysteresis observed in the PAI device is consistent, therefore, with deep electron trapping either at the interface or in the bulk of the insulator. The

Table 1
Parameters extracted for MIS devices in the dark and under illumination. N_A is the P3HT doping density, n_{ti} the additional trapped electron density obtained under illumination, with n_{tr} the residual density after illumination.

Device	N_A (cm^{-3})	n_{ti} (cm^{-2})	n_{tr} (cm^{-2})
PAI	2.3×10^{16}	2.5×10^{12}	5.6×10^{11}
SU-8	2.8×10^{16}	7.4×10^{11}	4.6×10^{11}
PSQ	5.3×10^{15}	4.1×10^{11}	2.3×10^{11}

effective interface density, n_t, of trapped electrons producing a shift, ΔV_{FB}, in the flatband voltage is given by Ref. [19].

$$n_t = \frac{C_I \Delta V_{FB}}{Aq}. \quad (3)$$

For the first voltage cycle applied to the PAI device, ΔV_{FB} is ~7 V, from which we estimate that during the forward sweep an effective concentration, $\sim 5.6 \times 10^{11}$ cm^{-2}, of electrons became deeply trapped at the interface. The dark, post-illumination plot showed a further shift in V_{FB} of ~5 V suggesting that the density of deep electron traps is at least $\sim 1 \times 10^{12}$ cm^{-2}.

As reported previously [17,19], the dark *C-V* plots of PSQ and SU-8 capacitors are reproducible and show no hysteresis even after illumination, suggesting that few, if any electrons are trapped/released within the timescale of the voltage sweep. However, after illumination, a significant positive shift in flatband voltage occurred showing that, even in these devices, deep electron traps exist with a density between 2×10^{11} and 5×10^{11} cm^{-2}. That these traps were not active during the initial voltage cycle, suggests that they are either new interface/insulator traps generated by an optical mechanism or existing traps that are only accessible to optically generated electrons. HMDS treatment of the PAI and PSQ layers has clear benefits in stabilising device properties [20,25]. However, even if the HDMS SAM remains immobilised on the insulator surface throughout the anneal process, the very different results in Fig. 2 suggests that the observed effects reflect the properties of the underlying insulator. This is not surprising since the blocking of interface electron traps on SiO_2, even by long-chain SAMs, is a only a temporary effect [28].

4.2. Photocapacitance response

Turning now to the photocapacitance measurements, we note that when MIS capacitors are in accumulation, the electric field in the bulk semiconductor is essentially zero and the insulator capacitance is fully charged. Hence, even if light-generated carrier species escape recombination/trapping in the P3HT, no further holes can accumulate at the interface and no change can occur in the measured capacitance.

When under illumination and driven into depletion, all the photocapacitance plots in Fig. 2 show some common features but also subtle, though important differences. In a depleted p-type semiconductor, band bending is such that photo-generated holes drift out of the depleted P3HT towards the gold contact while electrons drift to, and accumulate at the P3HT/insulator interface. To various degrees, under illumination, all the devices in Fig. 2 exhibit counter-clockwise hysteresis consistent with electron trapping at the P3HT/insulator interface causing a positive shift in V_{FB}. The minimum capacitance, C_{min}, also increases. This occurs either because V_{FB} shifts at the same rate as the voltage sweep rate due to rapid interface electron trapping [19] or because of the accumulation of free electrons, i.e. formation of an inversion layer, in the semiconductor at the interface [19,29,30].

The interface density of trapped electrons during illumination, n_{ti}, is estimated from equation (3) where ΔV_{FB} is taken as the difference in V_{FB} between the reverse voltage sweeps of the photocapacitance-voltage plots and the forward sweep of the pre-illumination *C-V* plots. Similarly, V_{FB} observed during the forward sweep of the post-illumination dark *C-V* plot yields the residual trapped electron density, n_{tr}. Table 1 lists the values of n_{ti} and n_{tr} determined for each device.

Below, we now consider the differences in the photocapacitance responses by taking each device in turn.

(a) PAI devices

PAI-based capacitors exhibited the largest shift in V_{FB} under illumination – even applying 40 V across the device was insufficient to deplete fully the P3HT. In this case, photo-generated electrons rapidly trap at the P3HT/PAI interface. Unlike the other cases, electron trapping occurred under conditions close to flatband, i.e. little or no band bending in the P3HT. Eventually, with $n_{ti} \sim 2 \times 10^{12}$ cm^{-2} no further trapping occurred. Thereafter, depletion set in and the *C-V* plots for both forward and reverse sweeps followed the dark response with minimal hysteresis but displaced along the voltage axis. After completing the reverse voltage sweep, i.e. biasing the device into accumulation, most, but not all, the trapped electrons rapidly de-trapped or were neutralised by holes. This is evidenced by the forward voltage sweep of the post-illumination *C-V* plot reproducing the pre-illumination reverse sweep data, so that $n_{tr} \sim 5.6 \times 10^{11} cm^{-2}$. The results suggest the presence of two types of interface trap: a set of deep traps represented by n_{tr} and shallow interface traps lying between the equilibrium Fermi level of P3HT and the electron QFL under illumination. Under illumination, shallow traps lying below the QFL become active and trap electrons photo-generated within a diffusion length of the interface. On terminating the illumination, the QFL falls below the trap energy, electrons rapidly de-trap and the device returns to its pre-irradiation state, except for the effect of more deeply trapped electrons.

Similarly large, light-induced shifts in V_{FB} were reported [17] for P3HT MIS capacitors based on polyimide, a polymer closely related to PAI. In that case, the large shift in V_{FB} was attributed to the electronegative character of polyimide. This is likely also to be the case here owing to the prevalence of C=O groups in the molecular structure of both polymers. The role of polar groups in interface electron trapping has been reported in phototransistors [12–14] as indicated in section 2 above.

(b) SU-8 devices

The photocapacitance plot for the SU-8 device differs in several respects from that for PAI. Initially, the capacitance in depletion follows that in the dark. Only when the P3HT is strongly depleted, i.e. significant band bending, does the plot depart from the dark values, becoming constant at a higher C_{min} ~325 pF. At first, the return plot rises only slowly – mainly due to the neutralisation of photo-generated free electrons, which are known to be present at the semiconductor/insulator interface in this device type [30].

Below ~15 V, the return *C-V* plot rises more rapidly albeit with a slightly shallower slope than seen in the forward sweep. While this could indicate that additional acceptor sites had been created in the P3HT during illumination, the behaviour is more likely to arise from the release of electrons from interface traps, resulting in the gradual relaxation of V_{FB} during the reverse voltage sweep. At flatband, an estimated 7.4×10^{11} electrons cm^{-2} remained trapped at the interface. The post-illumination dark response revealed that a residual density, n_{tr} $\sim 4.6 \times 10^{11}$ cm^{-2} of deeply trapped electrons remained in the device even after biasing into accumulation, when neutralisation by holes was expected.

(c) PSQ devices

Previously reported results for PSQ devices [17] were similar to that for the SU-8 device here. Now, due to the different curing protocol used, the photocapacitance plots were slightly different. Under illumination, the photocapacitance response followed the pre-illumination dark response almost to full depletion with C_{min} only marginally higher than

seen in the dark. A slight but clearly perceptible jump up in capacitance occurred following the first voltage decrement of the return voltage sweep. This suggests that the flatband voltage shifted by ~35 V during the forward sweep, corresponding to the trapping of $\sim 1 \times 10^{12}$ electrons cm^{-2} at the interface.

On reducing the voltage to ~20 V, approximately half of these electrons de-trapped or were neutralised within the timescale of the sweep. At flatband (~15 V) the number reduced even further, n_{ti} $\sim 4.1 \times 10^{11}$ cm^{-2}. As with PAI and SU-8, the post-illumination *C-V* response showed a residual, deeply trapped interface electron concentration with n_{tr} $\sim 2.3 \times 10^{11}$ cm^{-2}.

From the above, we see that photocapacitance measurements investigate directly the effects of interface trapping in MIS devices and are relevant, therefore, to the operation of organic phototransistors. In particular, the photocapacitance approach decouples interface trapping from other effects such as photoconduction and trapping in the bulk semiconductor that can influence the measured source-drain current in transistor structures.

4.3. Dynamic response

As seen with phototransistors, a light-induced change in V_T lends itself to photo-sensor applications in which case, the dynamic response is of importance. With MIS capacitors, two approaches are possible: (a) Bias the device into partial or even full depletion and with the voltage held constant measure the increase in capacitance under illumination and afterwards in the dark. This approach is discussed in section 4.4. (b) Bias the device into partial depletion, ideally to the steepest part of the *C-V* plot and use a PID feedback arrangement (see section 3.3 and Fig. 1(b)) to maintain a pre-set capacitance by adjusting the applied voltage both during and after illumination [17]. Maintaining a constant capacitance means that band bending (potential distribution) in the semiconductor should be invariant during the measurement. Furthermore, since the shift in voltage results from a shift in V_{FB}, it is also directly proportional to the density of trapped electrons at the interface. Thus, the observed signal also provides a means of investigating the dynamics of interface trapping unhindered by complications that could arise from time-varying changes in the degree of band bending. This is the approach described in this section.

Capacitors based on PSQ and SU-8 with *C-V* plots similar in profile to those shown in Fig. 2 (but with C_I (accumulation) designed to be ~175 pF) were exposed to successive 60 s periods of illumination with light of decreasing wavelength. The changes in voltage, ΔV, required to maintain constant capacitances of 160 pF (PSQ) or 165 pF (SU-8) were recorded and are shown in Fig. 3(a) and 4(a) respectively. Between each exposure, devices were left in the dark for 60 s while continuing to monitor ΔV. Since the intensity at different wavelengths could differ by up to ± 10% from the set value of 0.2 W/m^2 and to make comparisons more meaningful, the plots for each wavelength are normalised to the photon flux (photons/s) incident on the device.

As expected from the absorption spectrum of P3HT, only a minimal response was observed at 700 nm with the largest response occurring for wavelengths below 650 nm, the absorption edge of P3HT. Both under illumination and subsequently in the dark, the response was composed of a fast and a slow component. A similar pattern of behaviour is seen in Fig. 4 for a MIS capacitor in which the SU-8 layer thickness was increased to yield a *C-V* plot close to that for PSQ i.e. C_I ~175 pF and C_{min} ~130 pF.

As seen from the solid lines in Figs. 3 and 4, the responses can be fitted by double exponential relations, i.e. under illumination

$$\Delta V(t) = A_1\left(1 - e^{-\frac{t}{\tau_1}}\right) + A_2\left(1 - e^{-\frac{t}{\tau_2}}\right) \quad (4)$$

and subsequently in the dark

$$\Delta V(t) = B_1 e^{-\frac{t}{\tau_3}} + B_2 e^{-\frac{t}{\tau_4}} \quad (5)$$

where $A_{1,2}$ and $B_{1,2}$ represent the magnitudes of the processes and τ_n their time-constants for increasing and deceasing voltages. Parameter values used in fitting the curves in Figs. 3 and 4 are given in Tables 2 and 3, respectively.

Two distinct processes related to separate trapping states have been observed previously in the photo-response of pentacene transistors [31]. However, from a consideration of the equivalent circuit of an MIS capacitor - see the inset in Fig. 3(b) - we can predict the occurrence of an initial step change upon illumination, which is not necessarily linked to charge trapping. For low frequency operation, the partially depleted device in the dark may be represented by a series combination of the insulator capacitance, C_I, the depletion region capacitance, C_D, and the bulk resistance, R_S, of the P3HT. This state corresponds to switch, *S*, open. Upon illumination, photo-generated electron-hole pairs increase the conductivity of the depletion region, effectively closing *S* and introducing a resistance, R_P, in parallel with C_D.

Simple circuit analysis shows that, for a measurement at a fixed angular frequency, ω, the presence of R_P increases the device capacitance, *C*, according to the expression

$$C = \frac{C_I + \omega^2 C_I C_D (C_I + C_D) R_P^2}{(1 - \omega^2 R_S R_P C_I C_D)^2 + \omega^2 ((R_S C_I + R_P (C_I + C_D))^2}. \quad (6)$$

To maintain constant capacitance, the PID controller compensates by increasing the applied voltage, which in turn expands the depletion region, reducing C_D. On turning off the light, the reverse process occurs, switch *S* opens, device capacitance falls and is compensated by a decrease in applied voltage and increase in C_D. This being the case, time constants τ_1 and τ_3, should have similar values. In the present study, the faster process for both device types do indeed have similar time-constants, $\tau_{1,3} = 5.1 \pm 1.5$ s, and close to the response time of the PID controller.

Under illumination, the magnitude of R_P and hence its shunting effect will be determined by the efficiency of carrier generation in the depletion region. The greater the generation rate, the smaller is R_P and

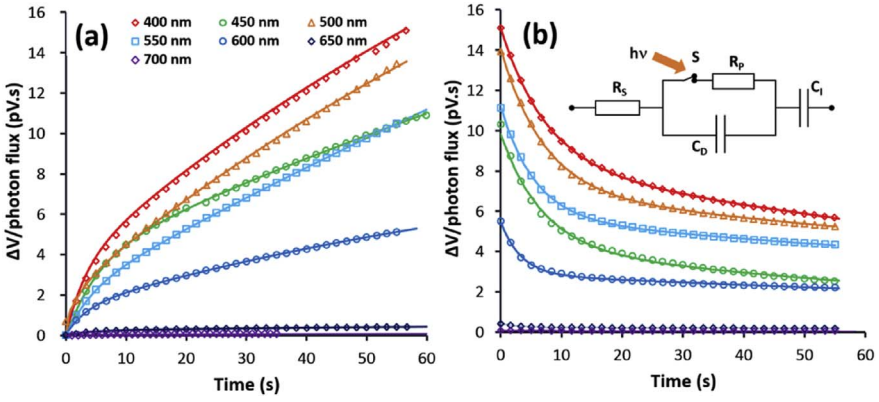

Fig. 3. Change, ΔV, in bias voltage needed to maintain the capacitance of a PSQ/P3HT capacitor constant at 160 pF (a) during illumination with 700 nm–400 nm light and (b) in the dark immediately after each exposure. The data points are normalised to the photon flux incident on the sample. Solid curves are double exponential fits to the data. The inset in (b) depicts the effect of illumination on the equivalent circuit of the device (see text for details).

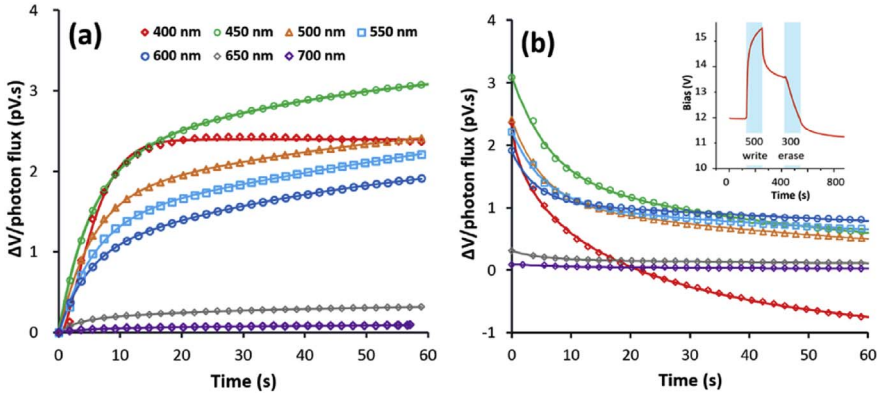

Fig. 4. Change, ΔV, in bias voltage needed to maintain the capacitance of a SU-8/P3HT capacitor constant at 165 pF (a) during illumination with 700 nm - 400 nm light and (b) in the dark immediately after each exposure. Solid curves are double exponential fits to the data points. The inset in (b) shows a write-erase cycle following successive exposures to 500 nm and 300 nm light.

Table 2
Parameters for the double-exponential fits of equations (4) and (5) to the PSQ/P3HT MIS capacitor data in Fig. 3.

λ (nm)	τ_1 (s)	τ_2 (s)	τ_3 (s)	τ_4 (s)	A_1 (pV.s)	A_2 (pV.s)	B_1 (pV.s)	B_2 (pV.s)
700	3.6	55	6.4	256	0.024	0.0913	0.0301	0.0599
650	3.1	57	2.6	189	0.214	0.319	0.18	0.241
600	3.3	92	3.3	199	1.26	8.54	2.62	2.86
550	4.3	367	5.6	203	2.06	60.4	5.58	5.64
500	7.5	257	7.1	196	2.28	56.3	7.14	6.93
450	5.2	218	6.7	109	3.71	30.5	5.62	4.23
400	3.3	121	7.3	141	3.3	31.8	6.78	8.36

Table 3
Parameters for the double-exponential fits of equations (4) and (5) to the SU-8/P3HT MIS capacitor data in Fig. 4.

λ (nm)	τ_1 (s)	τ_2 (s)	τ_3 (s)	τ_4 (s)	A_1 (pV.s)	A_2 (pV.s)	B_1 (pV.s)	B_2 (pV.s)
700	5.2	60.5	8.9	109	0.0424	0.0744	0.0490	0.0457
650	3.0	30.5	4.7	143	0.151	0.188	0.169	0.145
600	4.4	49.5	4.0	187	0.932	1.40	0.81	1.08
550	5.5	180	5.4	127	1.43	2.94	1.18	1.04
500	5.1	67.9	5.2	76.9	1.68	1.31	1.33	1.08
450	5.1	41.0	6.1	65	2.0	1.41	1.61	1.49
400	5.7				2.4			

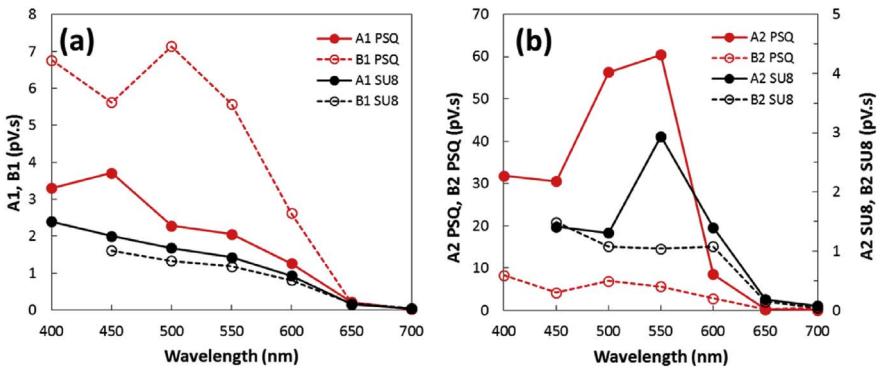

Fig. 5. Amplitudes of (a) the fast and (b) the slow processes during illumination (continuous lines) and subsequently in the dark (dotted lines).

the bigger the shunting effect. The resultant increase in the effective device capacitance then requires a greater increase in the compensating voltage, i.e. an increase in A_1. That A_1 rises by about two orders of magnitude between 700 and 600 nm is consistent with the increasing absorption in P3HT over this range, supporting the suggested mechanism for the 'fast' process.

As a further check of the mechanism, in Fig. 5(a) we plot the amplitudes, A_1, of the 'fast' processes under illumination and subsequently B_1, on turning off the light. For SU-8 both A_1 and B_1 are almost identical as would be expected from the equivalent circuit. For the PSQ device, which has an almost identical dark *C-V* plot, similar values should also be expected. This is indeed true for A_1 which is only slightly greater in the PSQ device than for SU-8. The significantly greater values for B_1 in PSQ, though, appear anomalous until we inspect the amplitudes of the 'slow' processes in Fig. 5(b).

Here we see that A_2 for PSQ is an order of magnitude greater than for the SU-8 device, contrary to values given in Table 1, where the more deeply trapped electron density induced by illumination in PSQ is slightly lower. The difference is explained by the experimental conditions. Values in Table 1 correspond to flatband, while the data in Figs. 4 and 5 correspond to partial depletion. We return to this point later.

Turning off the light effectively opens switch *S*. This immediately

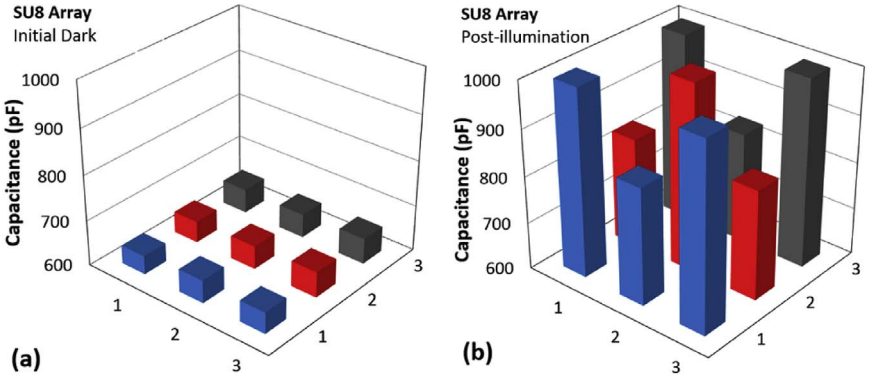

Fig. 6. SU-8 array capacitances measured in the dark (a) prior to and (b) immediately after illumination with white light. All measurements were made at 40 Hz and a bias of +5 V.

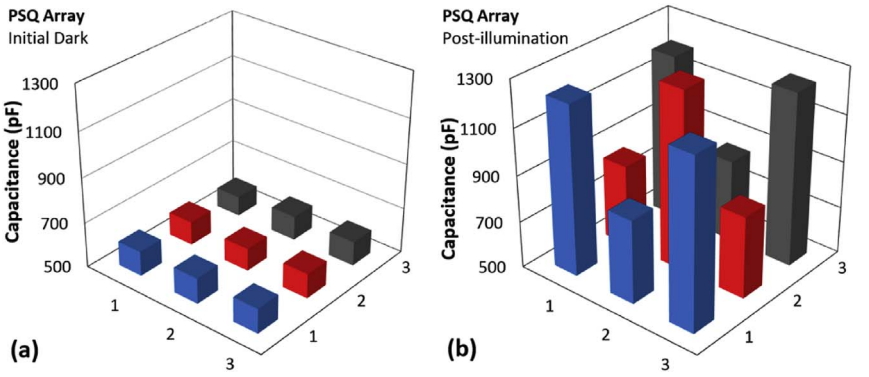

Fig. 7. PSQ array capacitances measured in the dark (a) prior to and (b) immediately after illumination with white light. All measurements were made at 40 Hz with a bias of +2 V.

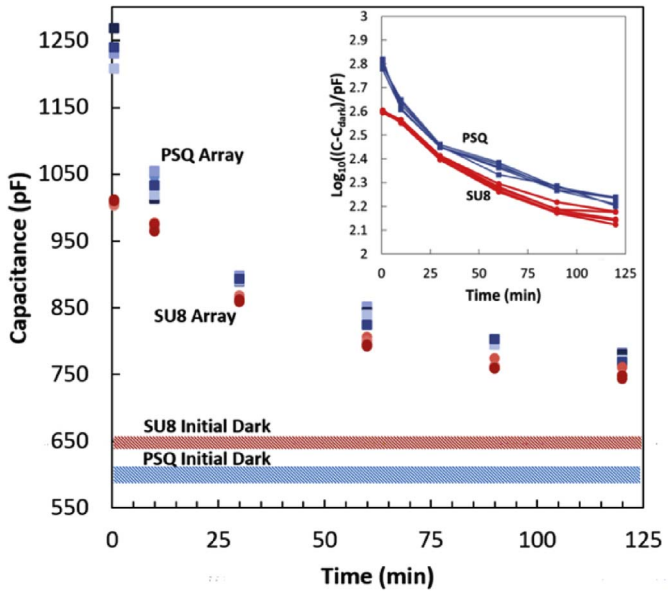

Fig. 8. Post-illumination relaxation of capacitances in the PSQ (squares) and SU-8 (circles) arrays. The shaded bands show the range of the initial dark values. The inset is a semi-log plot of the difference between the measured post-illumination capacitance and the dark values.

decreases the device capacitance as discussed earlier, which the PID controller counters by decreasing the applied voltage causing a reduction in band bending. This encourages the immediate release of a fraction of the trapped electrons, which for PSQ inflates the expected downward step size B_1. This effect is insignificant in the SU-8 device.

In Fig. 5(b), not only does the PSQ show a greater tendency to trap electrons compared with SU-8, but also a smaller fraction of these are released during the 60 s post-illumination period in the dark. During a measurement sequence, therefore, electrons accumulated at a faster rate at the PSQ interface than for SU-8. This may seem at odds with values of n_{ti} and n_{tr} given in Table 1. The apparent anomaly may be reconciled by noting that the constant capacitance approach only samples a limited band of interface traps with energies lying between the Fermi level and the QFL in depletion. Within this range, the trap densities may be very different in the two device types. Also, in section 3.2(c), it was pointed out that the trap concentration in PSQ may be as high as 1×10^{12} cm^{-2}, significantly higher than values in Table 1, which correspond to the shift in the *C-V* plot at V_{FB}.

Interestingly, while the response of the SU-8 device to 400 nm light still comprised a 'fast' element, the subsequent slow growth in ΔV was replaced by a decreasing contribution, which then continued during the light-off period. Further work is necessary to elucidate the mechanism, but the observation suggests an alternative approach to the memory effect demonstrated in phototransistors where illumination is used to 'write' data and briefly biasing the device into accumulation 'erases' the data [4,11,32,33]. Instead, the present work suggests that optical de-trapping may be feasible, as shown by the write-erase cycle in the inset of Fig. 4(b) where 500 nm light was used to write, i.e. trap electrons at the P3HT/SU-8 interface, and 300 nm light for erasing i.e. de-trapping the electrons.

As pointed out by Milvich et al. [11] time-constants associated with trapping processes are long compared to the response times of photodiodes. This is compensated, however, by the built-in amplification which allows measurable signals to be obtained in times much shorter than trapping time-constants. In MIS capacitors, charging of the gate capacitance also provides amplification via a charge-to-voltage conversion, allowing measurable voltage signals to be obtained in shorter times than required for trapping processes to reach equilibrium. Furthermore, the model proposed above for the fast transient provides a direct correlation between the measured voltage and the photocurrent optically induced in the semiconductor. This 'fast' signal is limited only by the response time of the comparator and feedback circuit.

4.4. Imaging application

The results presented in the previous sections suggest that organic MIS capacitors, in the same way as phototransistors, could be used as optical sensors or in imaging arrays. For such applications, the PAI/P3HT device combines good optical response with fast recovery when biased into accumulation. However, it is unstable under voltage cycling in the dark, in contrast to the stability of the other device types. For SU-8 and PSQ devices, the optical response is reasonable but, as seen in Fig. 2, sufficient electrons remain trapped at the interface post-irradiation in both cases for later off-line measurements of V_{FB} shifts or capacitance changes, either in single capacitors or in imaging arrays.

The feasibility of such an approach is demonstrated in Figs. 6 and 7, respectively, for SU-8 and PSQ MIS capacitor arrays. Initially, the full *C-V* plots of all the array capacitors were obtained. A typical example from each array is given in Fig. S1 (Supplementary Information). Then the capacitances of the central 3 × 3 array devices were recorded (Figs. 6(a) and 7(a)) in the dark at a voltage corresponding to the start of the C_{min} plateau (5 V for SU-8 and 2 V for PSQ devices). With the voltage still applied, the arrays were exposed to white light through the shadow mask shown in Fig. 1(d) and array capacitances re-measured in the dark (Figs. 6(b) and 7(b)) within the first minute after terminating the illumination.

Significant increases in capacitances, 70–100%, occurred in the pixels exposed to light, consistent with the shift in V_{FB} caused by trapping of photo-generated electrons. Some increase also occurred in the unexposed pixels. While there is a possibility that this may have been caused by electron transfer from the illuminated pixels as occurs in a charge injection device [30] this is unlikely owing to the much larger inter-pixel distances here. The most likely reason is a poor contact between the mask and substrate allowing light to leak to these pixels. This is confirmed by the data in Fig. S2 (Supplementary Information) obtained at a different time on a different array. No increase in capacitance occurred in the non-illuminated pixels. More importantly, though, the data shows also that the method can be used for on-line imaging as well as the off-line approach in Figs. 6 and 7.

As seen in Fig. 8, even 2 h after light exposure, the capacitances of the exposed pixels were still significantly higher than the initial dark values. The inset in Fig. 8 shows that, over this time scale, the decrease is not exponential. Rather it is described by a Kohlrausch distribution [31] indicative of electrons de-trapping from states distributed in energy. However, it should be noted that the decrease in capacitance will only provide a true measure of the decrease in trapped electron density when operating in the linear region of the *C-V* plot.

5. Conclusions

We have explored three ways in which MIS capacitors based on the p-type semiconducting polymer P3HT respond to light exposure. Irrespective of the approach taken, the underlying effect is the interface trapping of photo-generated electrons when the MIS capacitor is biased into the depletion regime of operation. The trapped electrons cause a shift in the flat-band voltage, V_{FB}, resulting in a positive shift of the *C-V* plot along the voltage axis, with little or no change in shape. In phototransistors, the effect would manifest itself as a shift in the threshold voltage, V_T, i.e. the so-called photovoltaic effect.

C-V plots obtained under illumination show rapid trapping and de-trapping of photo-generated electrons at the interface of the polar insulator PAI. This is consistent with the presence of electron traps initially lying just above the equilibrium Fermi level but below the light-induced electron quasi Fermi level (QFL). The responses of the SU-8 and PSQ devices again may be explained by interface electron trapping but this time in states with different de-trapping times. Differences between the insulators then result in differences in the *C-V* plots, e.g. magnitude of the hysteresis and shape of the return voltage sweep. *C-V* plots yield basic information, therefore, on the density of trapped electrons, both during and after light exposure.

The dynamic voltage response of devices held at constant-capacitance consisted of fast and slow components. We have shown that, as light is turned on, the former may arise from the shunting of the depletion region capacitance by photoconduction in that region. When the light is turned off, the reverse effect occurs but in the presence of strong electron trapping, the fast process can be augmented by rapid electron de-trapping. The slow component arises from trapping and de-trapping in slower states. Harnessing the fast signal could, in principle, provide an alternative approach to optical sensing, particularly if the response time of the measurement system is improved. Additionally, the constant capacitance approach interrogates states between the Fermi level and the QFL. In principle, by changing the set capacitance, i.e. the degree of band bending, the slow component could be used for exploring states in different regions of the bandgap.

In our final approach, capacitances were measured at constant voltage both during and after illumination. Significant capacitance increases occurred in the pixels exposed to light, again consistent with a shift in V_{FB} caused by trapping of photo-generated electrons. The enhancement in capacitance over that measured in the dark persisted for well over two hours thus providing the basis for off-line interrogation of an imaging array exposed to light.

Acknowledgements

EML, RFO, NA and JAG wish to acknowledge financial support from the Brazilian funding agencies FAPESP, CAPES, CNPq and the National Institute of Organic Electronics (INEO) which enabled visits to Bangor University to undertake the work reported here.

Appendix A. Supplementary data

Supplementary data related to this article can be found at http://dx.doi.org/10.1016/j.orgel.2017.10.010.

References

[1] K.-J. Baeg, M. Binda, D. Natali, M. Caironi, Y.-Y. Noh, Adv. Mater. 25 (2013) 4267.
[2] A. Pierre, A.C. Arias, Flex. Print Electron. 1 (2016) 043001.
[3] A. Pierre, A. Gaikwad, A.C. Arias, Nat. Photonics 11 (2017) 193.
[4] L. Zhang, T. Wu, Y. Guo, Y. Zhao, X. Sun, Y. Wen, G. Yu, Y. Liu, Sci. Rpts. 3 (2013) 1080.
[5] Y.-Y. Noh, D.-Y. Kim, K. Yase, J. Appl. Phys. 98 (2005) 074505.
[6] R. Liguori, W.C. Sheets, A. Facchetti, A. Rubino, Org. Electron. 28 (2016) 147.
[7] K. Wasapinyokul, W.I. Milne, D.P. Chu, J. Appl. Phys. 109 (2011) 084510.
[8] Y. Takanashi, K. Takahata, Y. Muramoto, IEEE Trans. Electron Devices 46 (1999) 2271.
[9] C.-S. Choi, H.-S. Kang, W.-Y. Choi, H.-J. Kim, W.-J. Choi, D.-H. Kim, K.-C. Jang, K.-S. Seo, IEEE Photonics Technol. Lett. 15 (2003) 846.
[10] H.-S. Kang, C.-S. Choi, W.-Y. Choi, D.-H. Kim, K.-S. Seo, Appl. Phys. Lett. 84 (2004) 3780.
[11] J. Milvich, T. Zaki, M. Aghamohammadi, R. Rödel, U. Kraft, H. Klauk, J.N. Burghartz, Org. Electron. 20 (2015) 63.
[12] H.-L. Park, I.-H. Lee, C.-M. Keum, S.-H. Lee, S.-D. Lee, Thin Sol. Films 619 (2016) 297.
[13] J. Kim, S. Cho, Y.-H. Kim, S.K. Park, Org. Electron. 15 (2014) 2099.
[14] Y. Chu, X. Wu, J. Lu, D. Liu, J. Du, G. Zhang, J. Huang, Adv. Sci. 3 (2016) 1500435.
[15] S.M. Sze, Physics of Semiconductor Devices, second ed., John Wiley and Sons, NY, 1981.
[16] E.H. Nicollian, J.R. Brews, MOS (Metal Oxide Semiconductor) Physics and Technology, Wiley-Interscience, 2002.
[17] D.M. Taylor, J.A. Drysdale, I. Torres, O. Fernández, Appl. Phys. Lett. 89 (2006) 183512.
[18] J. Lancaster, D.M. Taylor, P. Sayers, H.L. Gomes, Appl. Phys. Lett. 90 (2007) 103513.
[19] C.P. Watson, M. Devynck, D.M. Taylor, Org. Electron. 14 (2013) 1728.
[20] E.M. Lopes, R.S. Ywata, N. Alves, F.M. Shimizu, D.M. Taylor, C.P. Watson, A.J.F. Carvalho, J.A. Giacometti, Org. Electron. 13 (2012) 2109.
[21] H. Sirringhaus, N. Tessler, R. Friend, Synth. Met. 102 (1999) 857.
[22] E. Itoh, I. Torres, C. Hayden, D.M. Taylor, Synth. Met. 156 (2006) 129.
[23] D.M. Taylor, N. Alves, J. Appl. Phys. 103 (2008) 054509.
[24] I. Torres, D.M. Taylor, E. Itoh, Appl. Phys. Lett. 85 (2004) 314.
[25] I. Torres, D.M. Taylor, J. Appl. Phys. 98 (2005) 073710.
[26] D.M. Taylor, H.L. Gomes, A.E. Underhill, S. Edge, P.I. Clemenson, J. Phys. D Appl.

Phys. 24 (1991) 2032.
[27] M.L. Chabinyc, R.A. Street, J.E. Northrup, Appl. Phys. Lett. 90 (2007) 123508.
[28] L.-L. Chua, J. Zaumseil, J.-F. Chang, E.C.-W. Ou, P.K.-H. Ho, H. Sirringhaus, R.H. Friend, Nature 434 (2005) 194.
[29] M. Devynck, B. Rostirolla, C.P. Watson, D.M. Taylor, Appl. Phys. Lett. 105 (2014) 183301.
[30] C.P. Watson, D.M. Taylor, Appl. Phys. Lett. 99 (2011) 223304.
[31] M. Debucquoy, S. Verlaak, S. Steudel, K. Myny, J. Genoe, P. Heremans, Appl. Phys. Lett. 91 (2007) 103508.
[32] M.Y. Cho, S.J. Kim, Y.D. Han, D.H. Park, K.H. Kim, D.H. Choi, J. Joo, Adv. Funct. Mater. 18 (2008) 2905.
[33] K.H. Kim, S.Y. Bae, Y.S. Kim, J.A. Hur, M.H. Hoang, T.W. Lee, M.J. Cho, Y. Kim, M. Kim, J.-I. Jin, S.-J. Kim, K. Lee, S.J. Lee, D.H. Choi, Adv. Mater. 23 (2011) 3095.